Sensors for Legged Mobile Robots

Lino Marques, Jorge Lobo, Jorge Dias, Urbano Nunes, A. T. de Almeida,
Institute of Systems and Robotics
Department of Electrical Engineering
University of Coimbra, Portugal
{lino, jlobo, jorge, urbano, aalmeida}@isr.uc.pt

Abstract: The article presents a survey of sensors relevant for mobile robot navigation and their sensing principles. The sensors surveyed include range sensors, inertial systems and positioning systems. There are many applications, from different sectors that could profit from this type of technology: autonomous mobile platforms for materials handling in industry, warehouses, hospitals, etc.; forestry cutting and undergrowth management equipment; autonomous fire-fighting machines; mining machinery; advanced electrical wheel chairs; autonomous cleaning machines; security and surveillance robots. Advanced sensor systems which are now emerging in different activities from the health care services to the transportation sector and domestic services, will significantly increase the capabilities of autonomous vehicles and will enlarge their application potential.

1. Introduction

Walking mechanism have certain clear advantages in applications when the vehicle or robot has to move on rough terrain or in an environment which has been designed primarily for man, like buildings with stairs etc. All this mobility demands for more sensorial capabilities and more complex control strategies. Inertial sensors play here an important rule, giving the necessary information for navigation, and gait control.

Modelling the flexibility of walking machines is a complex problem and a correct set of sensors could conduct to good solutions. Acceleration sensors and gyrometers can be used to obtain the attitude/position of the machine's body and improve the design of robust algorithms to kept it level on both flat and irregular terrain, but also adapt the walking machine's gait for moving on an uneven terrain.

A remarkable variety of physical principles have been utilised in robot navigation. Some depend on receipt of information from somewhere outside the robot itself, and are therefore subject to error or in-operativeness, when such information is erroneous or is lacking, whether from natural or artificial induced sources. Others are based on internal sensing or dead-reckoning [1], and do not depend on external references, overcoming some of their associated problems, but having others, such as drift. These last systems provide relative position measurements and not absolute positioning. The present location of a robot is determined by advancing some previous position through known course and velocity information over a given length of time.

Inertial navigation systems depend on measurements carried out entirely within the robot, in accordance with the Newtonian laws of motion and gravitation. Therefore, by relying only on inertial sensor measurements, inertial systems are not affected by the robot's environment, making them non-jammable and self-contained. Mobile wheeled

---

[1]The origin of the term is "deduced reckoning" from sailing days.

robot dead-reckoning is usually associated with odometry, where encoders are used to measure wheel rotation and steering orientation. What at first might seem a simple and elegant solution turns out to be prone to errors, the most common source being wheel-slippage and different or irregular floors. Legged robots can also perform this dead-reckoning based on odometry from their joints, but will also be error prone. If legged robots are to be flexible, they have to navigate in unstructured environments, in which some navigation systems are inoperative or have their performance degraded, but where the self-contained inertial navigation system maintains its performance.

For outdoor robots the satellite based Global Positioning System (GPS) is currently available. The inertial system can provide short-term accurate relative positioning and GPS gives absolute positioning, bounding the error. The deduced reckoning of the inertial system is therefore combined with external reference absolute positioning provided by the GPS.

Range sensors have been also used for mobile robot navigation, and a wide set of applications could be found on [1] and [2]. Their information is very important for collision avoidance, map building, path finding and navigation.

2. Range Sensors

Range sensors in mobile robots are useful for navigation in unstructured and unknown environments, allowing to avoid obstacles, to detect landmarks and identify navigable routes. Humans use stereo vision for range sensing and environment perception, but this technique is not yet very appropriate for real time control of mobile platforms, because it is computionally intensive and unreliable. There are several techniques that can be used for mobile robotics range sensing, namely: magnetic, inductive, capacitive, ultrasound, microwave and optical techniques [1]. Magnetic range sensors can only be used to detect surfaces that generate magnetic fields so its utilization on mobile robotics is very limited. Inductive sensors can be used to measure distance to metallic surfaces, but its range is very short (more or less the diameter of the sensor coil) and its response depends on surface magnetic and conductive properties. On a similar way, capacitive sensors can be used to measure distances up to some centimetres to dielectric surfaces, but its response also depends on the surface dielectric properties.

The most commonly used range sensors in mobile robotics are ultrasound and optical range sensors. Ultrasound sensors are inexpensive and can measure distances up to several meters. Active optical range sensors based on the projection of optical radiation onto a scene can give fast and accurate results.

2.1. TOF (Time-of-Flight) Ultrasound Range Sensors

Ultrasound range sensors usually use an electrostatic transducer for both transmitting and receiving an ultrasound wave. The distance is obtained by measuring the TOF of the ultrasonic wave: initially the transducer works as a transmitter, emitting a train of energy pulses, and then changes to the receiver mode to detect the echo (or echoes when in multiple-echo mode) reflected by the target object. The time elapsed between transmission and reception of the ultrasonic wave, denoted t_{TOF}, is proportional to the distance $\boldsymbol{d}$ between the transducer and the target surface (see Figure1):

$$d = \frac{1}{2} \cdot c \cdot t_{TOF} \tag{1}$$

where $\boldsymbol{c}$ denotes the velocity of the ultrasound wave in the propagation medium. Typically these sensors measure distances ranging from $30\,cm$ till about $10\,m$.
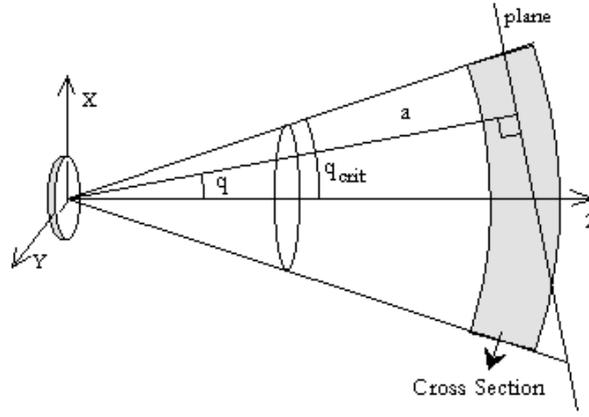
Figure 1. Ultrasonic TOF sensor model.

Ultrasonic transducers are commonly modeled by a flat piston of radius a vibrating at the resonant frequency f. When a voltage signal of frequency f is applied, an electrostatic force is exerted on the plastic foil of the transducer that begins vibrating and converts the electric energy in sound waves. The angular dependency of spatial pressure of the radiated waves can be modeled in terms of Bessel functions as follows:

$$P(\theta) = \frac{2 J_1(k \cdot a \cdot sin(\theta))}{k \cdot a \cdot sin(\theta)} \tag{2}$$

where $k = 2\pi/\lambda$ denotes the wave number of the sound field. The beam pattern that is produced has two distinct zones: the near zone, where the beam is contained within a cylinder of diameter $2a$, and the far zone where the beam diverges with half-angle θ_0 (correspondent to the main lobe of the radiation pattern). The divergence of the beam is a function of the ultrasonic wave frequency and transducers radius:

$$\theta_0 = arcsin\left(\frac{0.61\lambda}{a}\right) \tag{3}$$

The higher the frequency and the larger the radius, the narrower is the divergence angle. Figure 2 shows the far field radiation pattern, of a popular sonar sensor used in robotics (the Polaroid instrumented grade transducer). This sensor is composed by a circular piston with radius $a = 19\ mm$ and wavelength $\lambda = 6.95\ mm$, which corresponds an angle $\theta_0 \approx 12°$.

The information proceeding from a TOF ultrasound range sensor has an inherent uncertainty due to factors like: poor directionality that limits the accuracy in determining the spatial position of the environment features; possible misreadings and corruption of the data caused by multiple reflections and specularities. Although there are difficulties in the interpretation of sonar data owing to multiple specular reflections and the poor angular resolution, these difficulties can be minimized, for instance, by employing physical models for the reflection of sonar [3]. A major disadvantage of ultrasound sensing is its susceptibility to specular reflection, that is, the measured distance is due to the reflection from the surface normal. This gives the simple observation model of the sonar, depicted in Figure 1, which predicts that the echo comes from a curved shape volume, and so we will have uncertainty related to the sensors divergence angle. For an experimental range modeling of a popular sonar sensor see for example [4]. In spite of the afore-mentioned problems, their low cost and easy interface make them one of the most used range sensor for indoors mobile robotics.
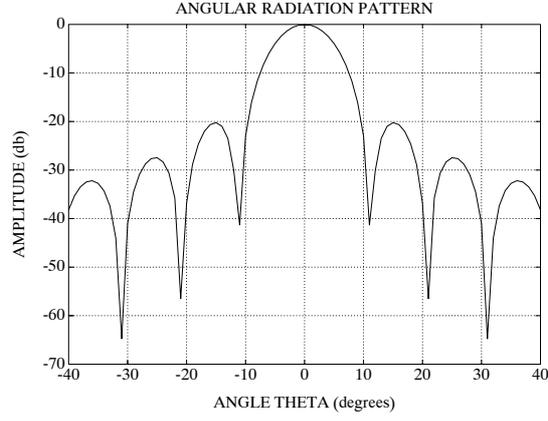
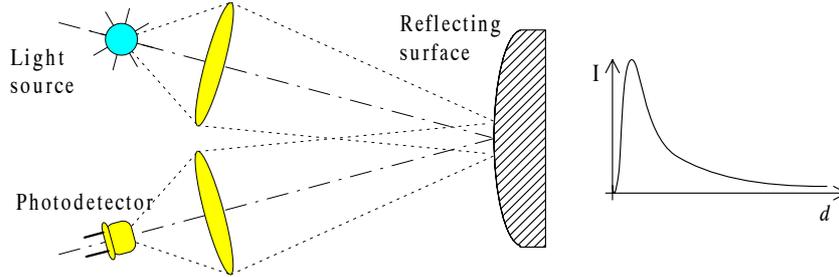Figure 2. Radiation pattern for the Polaroid transducer.

Figure 3. Reflective sensor principle. Some of the light emitted by the source is reflected on the surface and captured by the photodetector. The amount of captured optical light (I) depends on the distance (d) between the surface and the system.

2.2. Optical Range Sensors

Optical range sensors are particularly attractive for mobile robotics because they offer real-time accurate measurements with very high spatial resolution. These good properties are possible through the use of good quality optical components, namely coherent light sources (e.g. laser diodes) and very sensitive and high-resolution optical detectors (e.g. CCD cameras and avalanche photodiodes).

This section presents some of the most used optical range sensing methods in robotics, namely intensity reflection, triangulation, telemetry and lens focusing. Complementary surveys on optical range sensors can be found in the references [1, 5, 6].

2.2.1. Reflective Sensors

Return signal intensity sensors are composed by a light emitter and a photo-detector whose optical axes can be parallel for long range detection or convergent for shorter range detection (see Figure 3). These sensors measure the distance to an object by the amplitude of light reflected from the target surface. The amount of detected light reflected from the object surface can be expressed by the following equation:

$$\Phi = \int_S d\phi_r \qquad (4)$$

where $d\phi_r$ represents the flux received from an incremental object surface patch (see Figure 4). This flux can be expressed by:

$$d\phi_r = I(\theta_e) \cdot d\omega_i \cdot R \cdot d\omega_r \cdot \Re(\theta_d) \qquad (5)$$
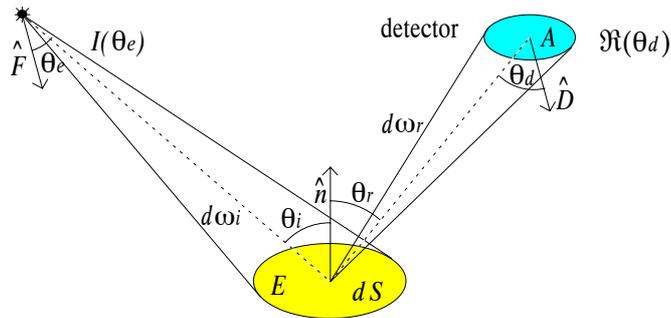
Figure 4. Reflection geometry used to calculate the detected intensity relative to an incremental surface patch.

where $I(\theta_e)$ is the emitted intensity of light from the solid angle $d\omega_i$, R is the function that characterize the reflectivity pattern of the surface, and $\Re(\theta_d)$ represents the acceptance of the photodetector at an off-axis angle θ_d. Any common surface has specular and lambertian reflective components, so that using a simple model, like Phong's model [7], we have the following expression for the surface reflectivity:

$$R = K_s.\delta(\theta_r - \theta_i) + K_d.\cos(\theta_r) \tag{6}$$

where K_s and K_d are coefficients for specular and lambertian components respectively.

For a sensor with parallel emitter and detector optical axes, the detected intensity varies approximately with the bi-quadratic inverse of the distance [8]. Because the reflected intensity depends heavily on the surface optical characteristics and on its orientation, these sensors suffer from low repeatability. Several manufacturers (e.g. SunX, Banner, Honeywell) provide low cost photoelectric detectors that detect surfaces up to about 1 meter. A common strategy to eliminate the influence of background light, is the utilization of a modulated infrared beam and appropriate optical and electrical filters.

Reflective sensors can be easily homebuilt with increased functionalities using LEDs and photodiodes. For example some researchers use the IR proximity system to establish data links between a community of mobile robots.

Some mobile robots use IR proximity sensors for short range (typically from a few centimeters to 1 meter), narrow beam sensing, together with ultrasound range sensors for medium range (typically from 30 centimeters to 10 meters), wide beam sensing. The fusion of both kinds of information improves the results [9, 10].

2-D Reflective Sensor

The ISR Reflex sensor [8] is a small reflective sensor designed to be used in close range sensing, namely in electrical grippers and legged robots. This sensor is composed by two photodiodes on opposite sides of a light emitting diode (see Figure 5a). This configuration allows measuring the orientation to a planar homogeneous surface by the difference between the detected intensities in the two photodiodes.

Two prototypes of this sensor were integrated on a parallel jaw gripper presented in Figure 5b) for object detection and pre-prehension gripper control. The presence of objects between the gripper fingers is detected by occlusion between the emitter of a finger and the two detectors of the other finger. With this sensorial information, the gripper can align with the object to be grasped and make a smooth transition from position control to contact force control.
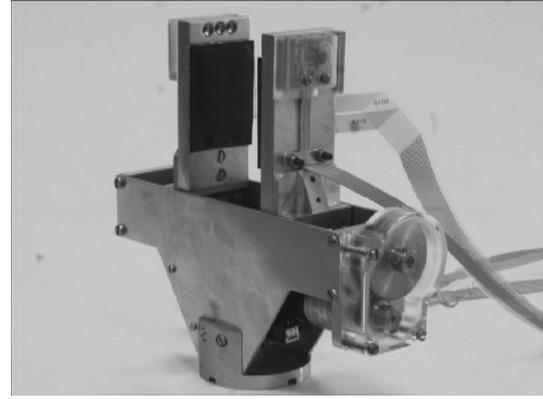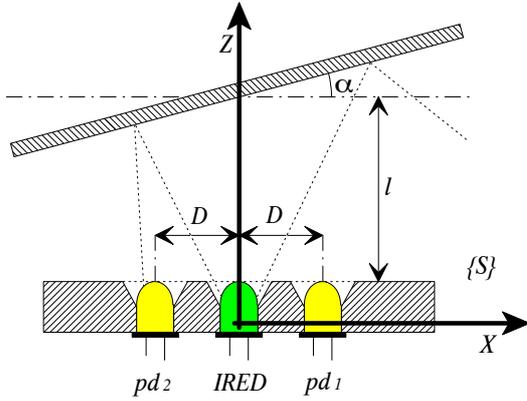
Figure 5. a) Geometry and elements of the proximity sensor. In the picture, pd_x is photo-detector x and $IRED$ is infrared light emitting diode. S represents the co-ordinated system associated to the sensor. b) *Gripper* with a reflective sensor on the extremity of each finger.

When used with planar homogeneous calibrated surfaces, the sensor can measure distances with an accuracy of 0.1 mm on a range from 5 to 100 mm. The orientation accuracy is about 0.1°.

Saw-tooth Modulated Reflective Array

The most commonly found commercial reflective devices are not intended to be used as full range measuring devices, but as simple non-contact presence detectors.

In[11] is described an efficient modulation method that can be used to build an array of reflective elements based on off-the-shelf infrared digital receivers. These receivers are mainly used in infrared data communication and have integrated in the same package a photodiode and the signal conditioning elements necessary to detect the serial bit stream. Each digital zero is transmitted as an infrared pulse typically modulated with a *40 kHz* frequency.

The method proposed to build the reflective array consists in modulating the emitted power in saw-tooth, so that each time the level of the reflected light reaches the receiver threshold, its state will go to TTL low. Because the saw-tooth emitted power is periodic, the receiver will generate a pulse width modulated signal (PWM) whose duty is a function of the distance to the surface. The digital nature of the receivers allow the easy integration of several reflective elements all controlled by an inexpensive microcontroller.

It was built a prototype based in this method with a range of about 1.5 m. This sensor can be very useful in reactive navigation, local map building and in target surface approaching.

2.2.2. Telemetry

Laser radar sensors or laser range-finders measure the distance ($\boldsymbol{d}$) between the sensor and a target surface based on the round-trip time (Δt) of a laser beam (see Figure 7). Considering $\boldsymbol{v}$ the velocity of the propagated wave on the medium, the distance $\boldsymbol{d}$ can be calculated by the following formula:

$$2d = v \cdot \Delta t \tag{7}$$

Although these sensors can use three different methods: pulse based time-of-flight (TOF), amplitude modulated (AMCW) and frequency modulated (FMCW), the first two
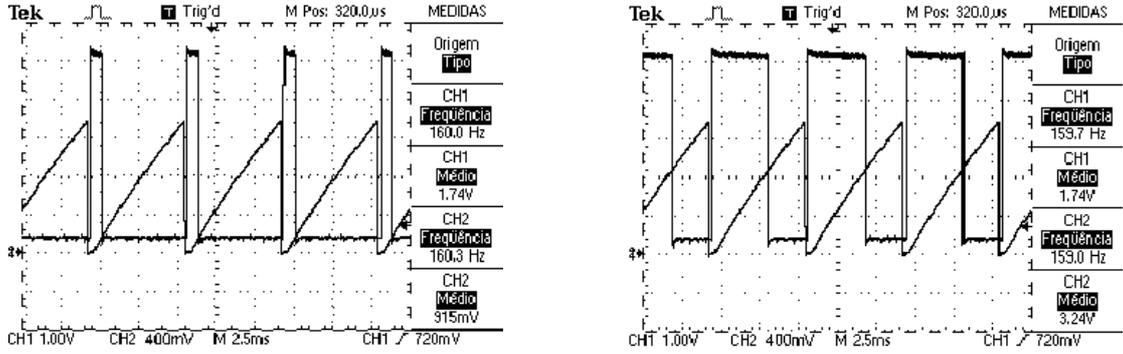
Figure 6. a) Emitted power (saw-tooth wave) and digital output wave for a surface 10 *cm* far from the sensor. b) The same, but for a 100 *cm* far surface.
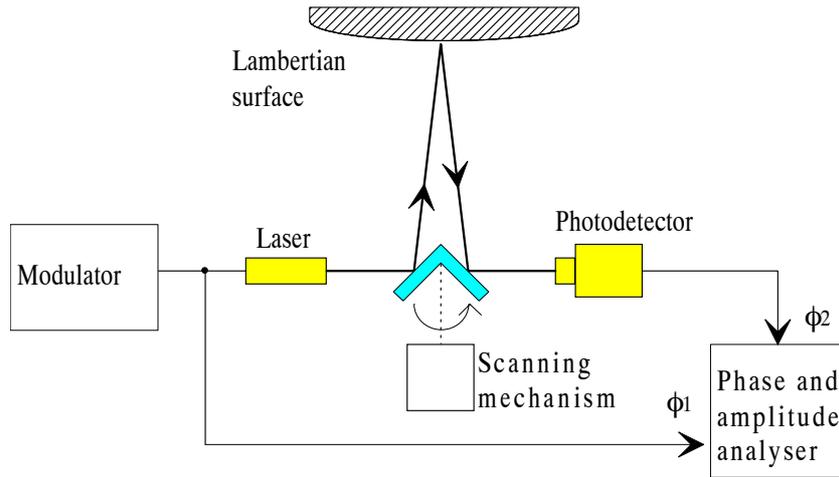

Figure 7. Laser radar. The distance is proportional to the round-trip time of a light pulse between the measuring system and a target surface.

are the most common ones. Pulsed rangefinders emit a short pulse of light and count the time to receive the reflected signal whilst AMCW range finders send an amplitude modulated continuous wave and use the phase shift between the emitted and the received wave to calculate the distance. Range accuracy of AMCW sensors depends upon the modulation wavelength and the accuracy with which the phase shift is measured. For round-trip distances longer than the modulation wavelength there will be ambiguity on the phase shift measurement.

Laser range-finders can measure not only the distance but also the amplitude of the reflected signal (intensity). The fusion of range and intensity images provided by scanning systems, can be helpful for image recognition tasks. These systems are fast, linear and very accurate over a long range of distances, but they are also the most expensive range sensors [12, 13, 14]. Table 1 presents the main characteristics of some currently available scanning systems [15, 16].

2.2.3. Triangulation

Triangulation sensors are based on the following trigonometric principle: *if the length of one side along with two interior angles of a triangle are known, then we can determine the length of the two remaining sides along with the other angle.*

An optical triangulation system can be either passive (use only the ambient light of the scene) or active (use an energy source to illuminate the target). Passive triangulation

Manufacturer	Model	Modulation	field of view	pixels	Accuracy	Min. dist.	Max. distance
Acuity Res.	AccuRange 4000	–	360°/line	2000	2.5mm	0	50 feet
ALST	ELRF-3-M	Pulsed/1Hz	–	1	2 m	50 m	30 km
ERIM	Adaptive Suspension	AMCW/14MHz	80° Az 60° El	128 × 128	3.9 cm	–	19.5 m
ERIM	Autonomous Land	AMCW/7MHz	80° Az 30° El	256 × 64	7.8 cm	–	39 m
ERIM	Intelligent Task	AMCW/720MHz	38° Az 38° El	256 × 256	2.5 mm	–	0.91 m
ERIM	US Postal Service	AMCW/700MHz	35° Az 35° El	300 × 300	0.05 mm	–	1 m
HDOS	Imaging Laser Radar	AMCW/15MHz	80° Az 60° El	~ 3000	0.15 m	–	460 m
IMRA	Laser Radar Sensor	–	90°/line	128	< 1 m	–	25 m
Leica	ODIN	–	6°sr	–	0.1 m	–	150 m
Odetics	GMS	AMCW/16MHz	60° Az 60° El	128 × 128	18 mm	–	> 10 m
Perceptron	LASAR	AMCW/varies	60° Az 60° El	1024 × 1024	2 mm	–	2-40 m
Riegl	LRI 20x5	Pulsed	5° Az 20° El	10.000	±3 cm	2 m	80 m
Riegl	LMS-Z210	Pulsed/20kHz	340° Az 80° El/	80/0.24 × 340/0.24	±2.5 cm	2 m	350m
Riegl	LD90-3300	Pulsed	–	1	±5 cm	3 m	400 m
Sandia	Scannerless R. Imager	AMCW/5.5MHz	ajustable	256 × 256	0.3 m	–	varies
Schwartz EO	LRF-200	Pulsed	360°/line	–	±30 cm	1 m	100 m
Schwartz EO	LADAR	Pulsed/9KHz	4° Az 10° El	25 × 65	0.3 m	–	500 m
Schwartz EO	Treesense	Pulsed/18KHz	2 × 90°	–	3 in	–	100 feet
Schwartz EO	Autosense II	Pulsed/15KHz	10° Az 30° El	30/line	3 in	2 feet	50 feet
Sick Optic	LMS200	Pulsed	180°/line	360/line	15 mm	–	150 m

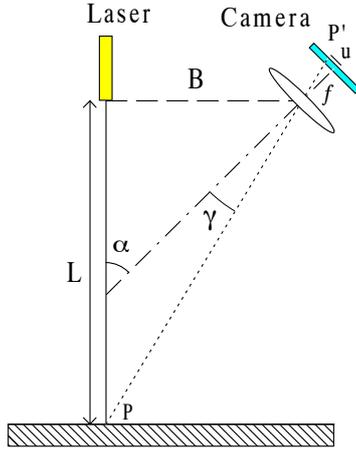Table 1. Main characteristics of some commercial laser rangefinders.

Figure 8. Triangulation system based on a laser beam and some kind of an imaging camera.

or stereoscopic systems use two cameras oriented to the same scene. The lens central points of each camera along with each point on the scene, define triangles with a fixed baseline (the distance between the central point of each camera lens) and variable interior angles. If the focal distance of each camera is known, these two interior angles can be calculated by the position of each point on both images. The main problem of these systems is the identification of corresponding points on both images (feature matching). To obtain a solution for this problem, active triangulation systems replace the second camera by a light source that projects a pattern of light onto the scene. The simplest case of such sensor, like the one represented in Figure 8, use a laser beam and a one-dimensional camera. The distance (L) between the sensor and the surface can be measured by the image position (u) of the bright spot formed on the interception point (P) between the laser beam and the surface:

$$L = \frac{B}{tan(\alpha - \gamma)} \tag{8}$$

where B is the distance between the central point of the lens and the laser beam (baseline) and α is the angle between the camera optical axis and the laser beam. The angle γ is the only unknown value in the equation, but it can be calculated using the position (u) of the image spot (provided that the value of the focal distance f is known):

$$\gamma = \arctan\left(\frac{u}{f}\right) \tag{9}$$

If it is required to obtain a range image of a scene, the laser beam can be scanned or one of several techniques based on the projection of structured light patterns, like light strips [17], grids [18, 19, 20], binary coded patterns [21, 22], color coded stripes [23, 24], or random textures [25] can be used. Although these techniques improve the performance of the range imaging system, they may also present some ambiguity problems [26, 27].

Triangulation systems present a good price/performance ratio because they are not very expensive, are pretty accurate, and can measure distances up to several meters. The accuracy of these systems decreases with the distance, but usually this is not a great problem in robotics because high accuracy is only required in close proximity to the objects. Otherwise it is enough to detect the presence of obstacles. The main problems of
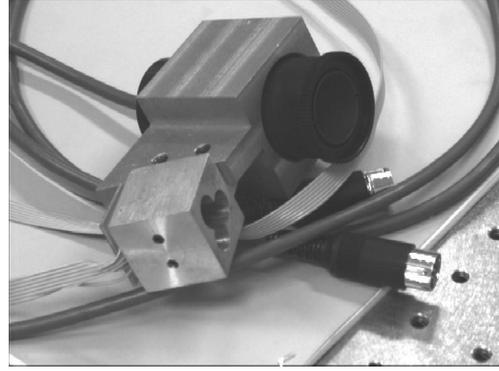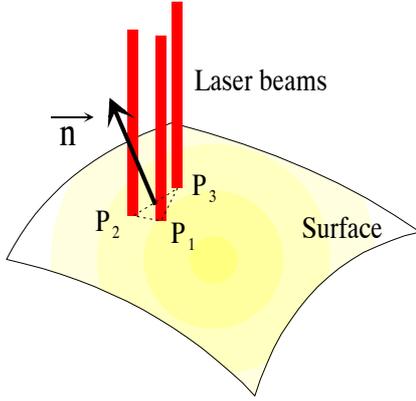
Figure 9. a) Distance and orientation measuring with three laser beams and a Position Sensitive Detector. b) Prototype of the Opto3D measuring head.
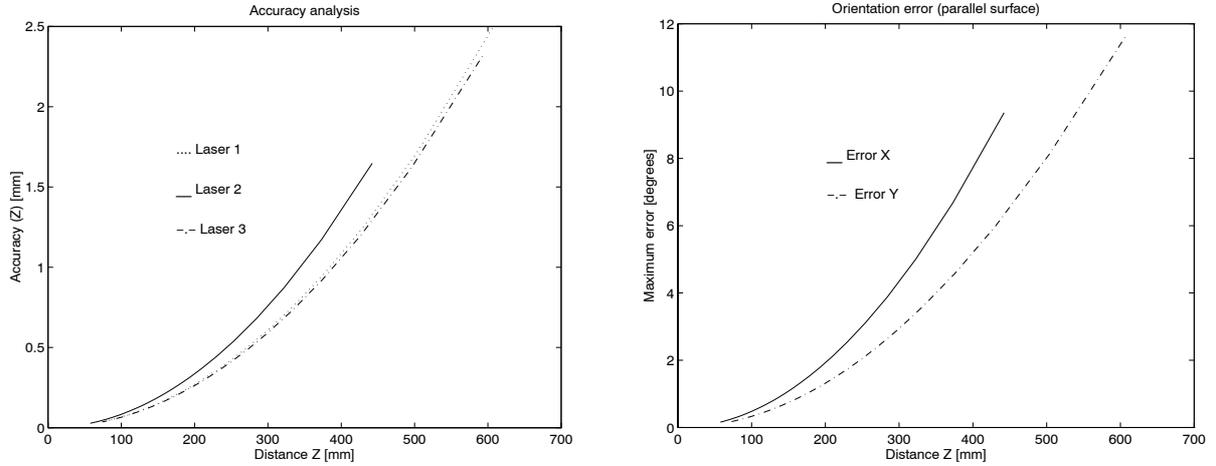

Figure 10. a) Distance accuracy vs. range. b) Angular accuracy for a perpendicular surface.

triangulation systems are the possibility of occlusion, and the possibility of misreadings in cases of specular surfaces that can blind the sensor or give rise to wrong measures because of multiple reflections [28, 29, 30, 31].

Opto3D

The Opto3D system is a triangulation sensor that uses a PSD[2] camera and three laser beams. The sensor measures the coordinates of the three interception points P_1, P_2 and P_3 (see Figure 9a), in order to calculate the orientation $\vec{n}$ of the surface:

$$\vec{n} = \overrightarrow{P_1P_2} \wedge \overrightarrow{P_1P_3} \tag{10}$$

The Opto3D sensor can measure distances from 5 cm up to 75 cm with accuracies from 0.05 to 2 mm (see Figure 10) [28, 29]. Like every triangulation sensor, the accuracy degrades with the distance. This sensor can measure orientation on a broad range with an accuracy better than 0.1°. The maximum orientation depends on the reflective properties of the surface (usually only a little amount of light can be detected from light beams that follow over almost tangential surfaces).
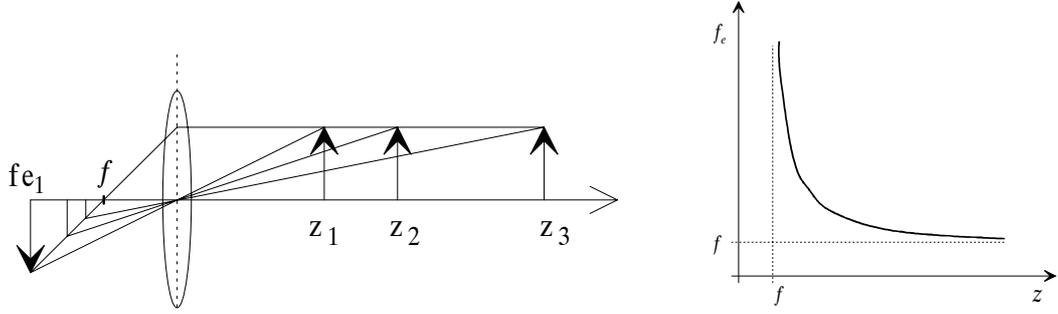
Figure 11. Using the Gauss lens law, it is possible to extract range information from the effective focal distance of an image.

2.2.4. Lens Focusing

Focus range sensing relies on Gauss thin lens law (equation 11). If the focal distance (f) of a lens and the actual distance between the focused image plane and the lens center (f_e) is known, the distance (z) between the lens and the object can be calculated using the following equation:

$$\frac{1}{f_e} = \frac{1}{f} - \frac{1}{z} \tag{11}$$

The main techniques exploring this law are **range from focus** (adjust the focal distance f_e till the image is on best focus) and **range from defocus** (determine range from image blur).

These techniques require high frequency textures, otherwise a focused image will look similar to a defocused one. To have some accuracy, it is fundamental to have very precise mathematical models of the image formation process and very precise imaging systems [32].

Image blurring can be caused by the image process or by the scene itself, so depth from defocus technique, requires the processing of at least two images of an object (which may or may not be focused) acquired with different but known camera parameters to determine the depth. A recent system provides the required high-frequency texture projecting an illumination pattern via the same optical path used to acquire the images. This system provide real-time (30 Hz) depth images (512×480) with an accuracy of approximately 0.2% of the distance range [33].

The accuracy of focus range systems is usually worse than stereoscopic ones. Depth from focus systems have a typical accuracy of 1/1000 and depth from defocus systems 1/200 [32]. The main advantage these methods is the lack of correspondence problem (feature matching).

3. Inertial Navigation and Inertial Sensors

The principle of generalised relativity of Einstein states that only the specific force on one point and the angular instantaneous velocity, but no other quantity concerning motion and orientation with respect to the rest of the universe, can be measured from physical experiments inside an isolated closed system. Therefore from inertial measurements one can only determine an estimate for linear accelerations and angular velocities. Linear velocity and position, and angular position, can be obtained by integration [34].

---

[2]Position Sensitive Detector

Inertial navigation systems implement this process of obtaining velocity and position information from inertial sensor measurements. The basic principle employed in inertial navigation is therefore deduced reckoning. A set of three accelerometers are used to measure acceleration along three orthogonal axes, and their outputs are integrated twice to determine position. To compensate body rotation, three gyroscopes are used to measure rotation rates about three orthogonal axis. In gimballed systems the accelerometers are kept on a gyro-stabilised platform with a high-speed rotor keeping the spatial orientation constant. In strap-down systems all sensors are rigidly fixed to the vehicle and the gyro data is used to transform the accelerometer data to navigation frame of reference. This can be seen as computationally stabilised accelerometer platforms, as opposed to the physically stabilised platforms used in gimballed systems.

Early versions of INS (Inertial Navigation Systems) were used by the Peenumüde group in Germany, in World War II, to guide the V2 rocket. This was one of the first examples of inertial guidance, relying on a gyro assembly to control the missile's attitude and an integrating accelerometer to sense accelerations along the thrust axis.

INS have since become widespread used in avionics, naval and some terrestrial applications. High-grade INS were firstly based on gimballed systems, relying on expensive inertial grade mechanical components. But these systems are typically high-cost, since they require high-grade sensors to overcome the severe drift problems due to the double integration of acceleration measurements to determine position and require precise calibration procedures. Although their cost has lowered due to technological developments, it is still rather high for robotic applications.

With recent sensor development and increased microprocessor performance, strap-down systems are becoming more accurate and suitable for high-end applications. They can provide good performance and reliability at a lower cost, consume less power and are more compact and lightweight [35].

Recent development in accelerometers and gyroscopes technologies has lead to some new low-cost sensors, as described in the following section. Strap-down systems based on these low-cost inertial sensors offer performance suitable for mobile robotic applications. The inertial system can be used to provide short-term accurate relative positioning, which combined with some other external reference absolute positioning system, to limit the INS absolute position drift error, will provide a suitable navigation system. Complete INS systems have to consider several factors such as the earth's rotation, and compensate for it in the calculations. But for mobile robotic applications, not travelling long distances along the earth's surface, some simplifications can be made [34].

Gyroscopes and accelerometers are known as inertial sensors since they exploit the property of inertia, i.e. resistance to a change in momentum, to sense angular motion in the case of the gyro, and changes in linear motion in the case of the accelerometer. Inclinometers (also known as clinometers, tilt sensors or level sensors) are also inertial sensors. They measure the orientation of the gravity vector, or to be precise, the resultant acceleration vector acting upon the sensor. In the following sections we will describe a few of these currently available low-cost sensors.

3.1. Accelerometers

A simple accelerometer may be conceived as a basic mass-spring system. The device is just a force-measuring instrument which solves the equation

$$F = ma \tag{12}$$

where m is the mass and a acceleration of the sensor, including gravity.

Practical accelerometers vary in design and technology, but all mechanise the equation $F = ma$ in some way. They can be electromagnetic, vibrating string, gyro-pendulum, optical, piezoresistive, piezoelectric, capacitive, amongst others. See [36] and [37] for an overview of some of the older accelerometer technologies.

3.1.1. Silicon Accelerometers

In recent years micro-machined accelerometers have become widely available, largely due to the ability to produce them at low cost. The needs of the automotive industry, namely for airbag deployment systems, encouraged silicon sensor development, enabling the batch-fabrication of the integrated accelerometer sensors. The current commercially available silicon accelerometers incorporate amplification, signal conditioning and temperature compensation. There are presently three main types of micro-machined low cost accelerometers. These are the capacitive, piezoelectric and piezo-resistive types. The piezoelectric sensors have no DC response, making them unsuitable for inertial navigation systems. In the piezo-resistive sensors the acceleration causes a sensing mass to move with respect to a frame, creating stress in a piezo-resistor, which changes its resistor value. The capacitive sensors rely on the displacement of capacitive plates due to the acceleration, creating a mismatch in the capacitive coupling. This change is used to generate a signal proportional to the acceleration applied to the sensor. Some recent devices are open loop sensors, others have a force balancing feedback loop that keeps the sensing element at its central position, gaining improved linearity. These devices are built so as to have a sensing axis and reduced off-axis sensitivity. Some are three-axial, incorporating three accelerometers in one sensor, simplifying mounting and alignment. These sensors present different measurement ranges from $\pm 2\,g$ up to $\pm 500\,g$.

Typical applications of such devices in the automotive industry include frontal impact airbag systems, suspension control, braking control and crash testing. They also find applications in industrial vibration monitoring, transportation shock monitoring and motion control. This big market will push the development of the technology further, and improved performance and lower cost sensors are to be expected.

A silicon accelerometer typically has a silicon spring and a silicon mass. In open loop configurations the acceleration is computed by measuring the displacement of the mass. Typical errors include: non-linearity of the spring; off-axis sensitivity; hysteresis due to the springs or hinges; rotation-induced errors (i.e. when body rotation adds rotational acceleration to the linear acceleration we intend to measure); and accelerometer signal noise.

For higher precision, force balancing closed loop configurations are implemented. Forces are applied to the mass to make it track the frame motion perfectly, and thus zero-balance the mass. Typical restoring forces used in silicon accelerometers include magnetic, piezoelectric and electrostatic. The sensor output will be given by the amount of force necessary to zero-balance the mass. By zero-balancing the mass, errors due to distortions and spring non-linearity are minimised. The input dynamic range and bandwidth is increased. Weaker hinges can be used, reducing hysteresis effects, and mechanical fatigue is minimised. No damping fluid is required, allowing operation in vacuum, and mechanical resonance avoided. Improved precision is thus accomplished.

In order to sense the proof mass displacement, either to directly give the output signal or control the zero-balancing loop, a number of sensing techniques are available. These include piezo-resistive, piezoelectric, capacitive and optical. The piezoelectric accelerom-

eters rely on the deposition of a piezoelectric layer onto the silicon springs. They have a high output at relatively low current, but have high impedance and no DC response. Optical silicon accelerometers rely on the changing characteristics of an optical cavity, due to mass displacement. Radiation penetrating the cavity is band-pass dependent of the mass displacement. This technology has been used in high-resolution, but rather high cost, pressure sensors [38]. Piezo-resistive and capacitive both have DC response and relatively low cost, making them suitable for low-grade inertial navigation systems.

Piezo-resistive Accelerometers

The first silicon accelerometer prototype was built in 1976 [38]. This device had a single cantilever structure, was fragile and had to be damped with a liquid. Despite its limitations it represented a significant step from the attachment of silicon strain sensors onto metal diaphragms, to having the resistor diffused onto single-crystal silicon. The basic design structures that have evolved for silicon are shown in figure below 12.
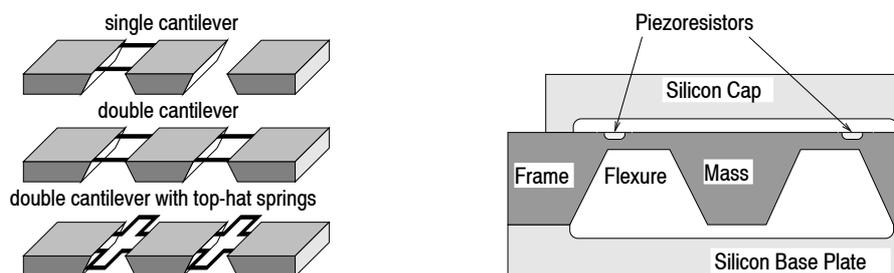

Figure 12. Design structures for the piezo-resistive accelerometer and cross-section of double cantilever sensor (adapted from [39]).

The single cantilever has, in theory, the highest sensitivity, but has more off-axis errors and is rather fragile. The double cantilever provides good off-axis cancellation and is more robust. The folded springs of the top-hat configuration allow for large displacements in a smaller area, thus reducing the cost of the sensor. An example of a double cantilever silicon accelerometer is the 3145 model from ICSensors.

Capacitive Accelerometers

In capacitive accelerometers, proof mass displacement alters the geometry of capacitive sensing elements.

One design of capacitive silicon accelerometers uses a main beam that constitutes the proof mass, with springs at each end. The beam has multiple centre plates at right angles to the main beam that interleave with fixed plates attached to the frame on each side, forming a comb-like symmetric structure. This design allows sensing of positive and negative acceleration along the axis of the main beam in the sensor plane.

Each of the centre plates fits between two adjacent fixed plates, forming a capacitive divider, as shown in figure 13. The two fixed plates are driven with an equal amplitude but opposite polarity square wave signals.

With no acceleration, the two capacitances are approximately equal and the centre plate will be at approximately zero volts. Any applied acceleration causes a mismatch in plate separation which results in greater capacitive coupling from the closer fixed plate; a voltage output can thus be detected on the centre plate. The acceleration signal is contained in the phase relative to the driving signal, thus a synchronous demodulator technique is actually used to extract the relatively low frequency acceleration signal.
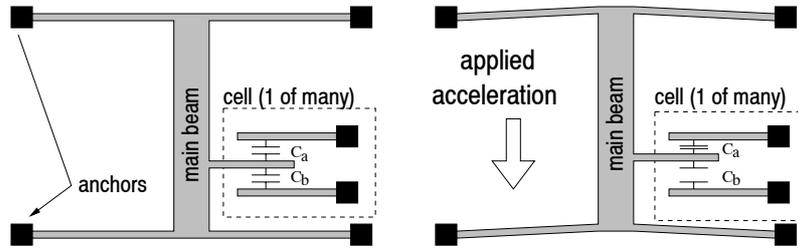
Figure 13. Capacitive comb finger array accelerometer working principle (adapted from [40]).

The resulting acceleration signal is used in a feedback loop to force balance the sensor, impeding the deflection and servoing the sensor back to its 0 g position. The balancing force is obtained electrostatically, caused by driving the centre plates to a voltage proportional to the acceleration signal. The force balancing servo loop response has to be fast enough and flat enough to track fast level changes, keeping the sensor nearly motionless, minimising the errors.

One example of a capacitive micro-machined accelerometer is the ADXL05 from Analog Devices Inc., a ± 5 g version of the ADXL50 ± 50 g accelerometer currently used in airbag deployment systems [41].

Other designs have also been implemented, namely the C3A-02 model from British Aerospace Systems and Equipment Ltd.. The three-axis accelerometer uses a single proof mass and capacitive sensing. This micro-machined sensor is not flat like the ones described above, and consists of a proof mass with multiple capacitive sensing elements, as shown in figure 14.
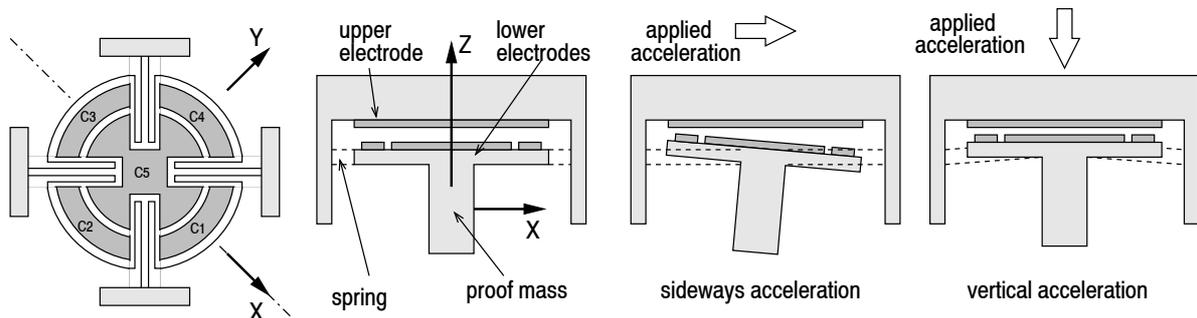

Figure 14. Diagram of BASE C3A-02 sensing element (adapted from [42]).

The difference between C1 and C3 capacitance values gives the x-axis acceleration, likewise C2 and C4 provide the y-axis acceleration and change in the capacitance value of C5 gives the z-axis acceleration [42].

3.2. Inclinometers

Though not strictly accelerometers, inclinometers or clinometers, measure the orientation of the resultant acceleration vector acting upon the vehicle. If the vehicle is at rest this means its orientation with respect to level ground. The AccuStar electronic capacitive inclinometer, from Lucas Sensing Systems Inc, is an example of such a device.

The concept of the sensor is based on a dielectric fluid, with an air bubble, inside a capacitive sensor. When the sensor is tilted the bubble, moving under the force of gravity, changes the capacitance of the sensor elements. The resulting differential generates an output signal which reflects the relative tilt in the sensing axis as shown in figure 15.
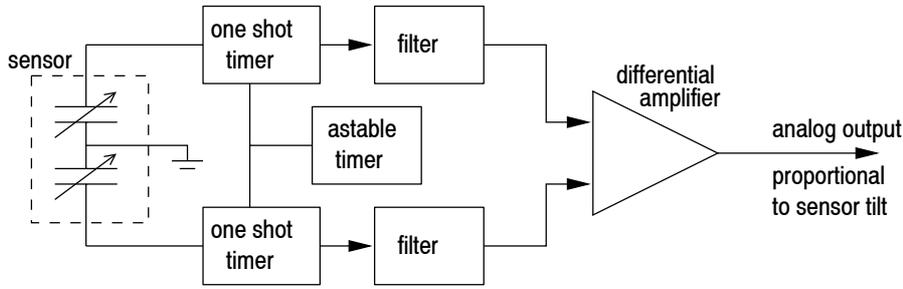
Figure 15. AccuStar inclinometer block diagram.

Due to the fluids inertia and settling time, and sometimes the measurement method, inclinometers tend to have a delayed response.

An interesting variation of this design is the dual axis inclinometer. The dielectric fluid with the air bubble is placed inside a dome shaped capacitive sensor. The sensing dome is divided into four quadrants. When the sensor is tilted, the bubble, moving under the force of gravity, changes the capacitance of the sensor elements in each quadrant. The resulting differential generates an output signal which reflects the relative tilt of the device in either x- or y-axis.

Other designs, still using the principle of the spirit level, measure resistance to obtain the tilt. These sensors has a suitably curved tube, with an electrically conducting liquid and gas bubble inside, and three electrodes. When the sensor is tilted the bubble's position relative to the electrodes changes, causing a difference in the electrical resistance between electrodes proportional to the tilt.

When using inclinometers care should be taken when accelerations other than gravity are present, since the tilt will be measured relative to the resultant vector. If the sensor is tilted by an angle α to the horizontal and is subject to an acceleration a in a direction normal to the sensor's measuring axis in the horizontal plane, the tilt sensor will not measure α. The measured angle will be

$$\alpha_{measured} = \alpha + \tan^{-1}\left(\frac{a}{g}\right) \tag{13}$$

where g is the modulus of the gravity vector [43].

Other inclinometer sensors use accelerometers as the sensing device, and either give an analog output corresponding to the sine of the angle or provide a linearized response. Crossbow's tilt sensors use this approach.

3.3. Gyroscopes

The mechanical gyroscope [3], a well known and reliable but expensive rotation sensor, based on the inertial properties of a rapidly spinning rotor, has been around since the early 1800s. The spinning rotor or flywheel type of gyroscope uses the fundamental characteristic of the angular momentum of the rotor to resist changing its direction to either provide a spatial reference or to measure the rate of angular rotation [35]. Many different designs have been built, and different methods used to suspend the spinning wheel. See [36] for some examples of such devices.

Optical gyroscopes measure angular rate of rotation by sensing the resulting difference in the transit times for laser light waves travelling around a closed path in opposite

---

[3]from the Greek word *gyros* meaning rotation and *skopein* meaning view.

directions - see figure 16. This time difference is proportional to the input rotation rate, and the effect is known as the 'Sagnac effect', after the French physicist G. Sagnac. Sagnac, in fact, demonstrated that rotation rate could be sensed optically with the Sagnac interferometer as long ago as 1913 [35].
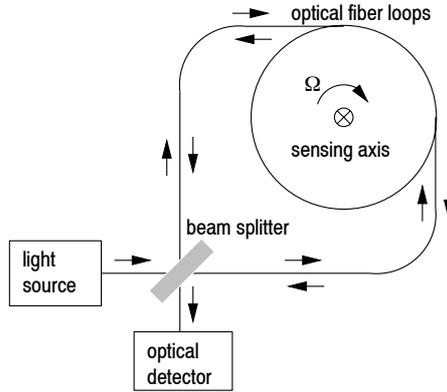

Figure 16. Simplified diagram of optical fibre gyroscope (adapted from [44]).

The communications industry has made optical fibres increasingly available, enabling the construction of low-cost fibre optic gyroscopes. These devices, named FOG or OFG for short, use multiple loops of optical fibre to construct the closed loop path, and semi-conductor laser diodes for the light source. A simplified diagram is shown in figure 16. The beam splitter divides the laser beam into two coherent components. The difference of travelling time between the two beams, caused by the difference in optical path lengths, is detected as the interference between the two beams by an optical detector. Several manufactures had produced relatively inexpensive optical fiber gyros for car navigation systems.

But even lower cost, and becoming increasingly compact are the vibrating structure gyroscopes. These use the Coriolis effect whereby an object with linear motion in a rotating frame of reference, relative to inertial space, will experience a so called Coriolis acceleration given by

$$\vec{a}_{coriolis} = 2\vec{\varpi} \times \vec{v} \tag{14}$$

where $\vec{\varpi}$ is the angular velocity of the rotating frame and the object's velocity $\vec{v}$ is given in the rotating frame of reference. Imagine a ball rolling across a rotating table. An outside observer would see it moving along a straight line. But an observer on the table would see the ball following a non-linear trajectory, as if a mysterious force was driving it. This apparent force is called the Coriolis force. You can see from equation 14 that the Coriolis force will be perpendicular to both the rotation axis and the objects linear motion.

3.3.1. Vibrating Structure Gyroscopes

The basic principle of Vibrating Structure Gyroscopes (VSG), is to have radial linear motion and measure the Coriolis effect. If a sensing element is made to vibrate in a certain direction, say along the x-axis, rotating the sensor around the z-axis will produce vibration in the y direction with the same frequency. The amplitude of this vibration is determined by the rotation rate. The geometry used takes into account, amongst other factors, the cancelling out of unwanted accelerations.

The common house fly, in fact, uses a miniature vibrating structure gyro to control its flight. A pair of small stalks with a swelling at their ends constitute radially oscillating

masses that will be subject to Coriolis forces when yaw is experienced. These forces will generate muscular signals that assist the acrobatic fly [1].

The Vibrating Prism Gyroscope

The Gyrostar ENV-011D, built by Murata MFG. Co. Ltd., is a a piezoelectric vibrating prism sensor. The device' s output is a voltage proportional to the angular velocity. The principle of the sensor is outlined in figure 17. Inside the device there is an equilateral triangle prism made from *elinvar*, elastic invariable metal, which is fixed at two points. Three piezoelectric ceramic elements are attached to the faces of prism, one on each side. The prism is forced to vibrate by two of the piezoelectric elements, whilst the other is used for feedback to the drive oscillator. These two elements are also used for detection. When there is no rotation they detect equally large signals. When the prism is turned, Coriolis forces will affect the prism vibration and the sensing piezoelectric elements will receive different signals. The difference between the signals is processed by the internal analogue circuits to provide an output voltage proportional to the angular velocity [45].
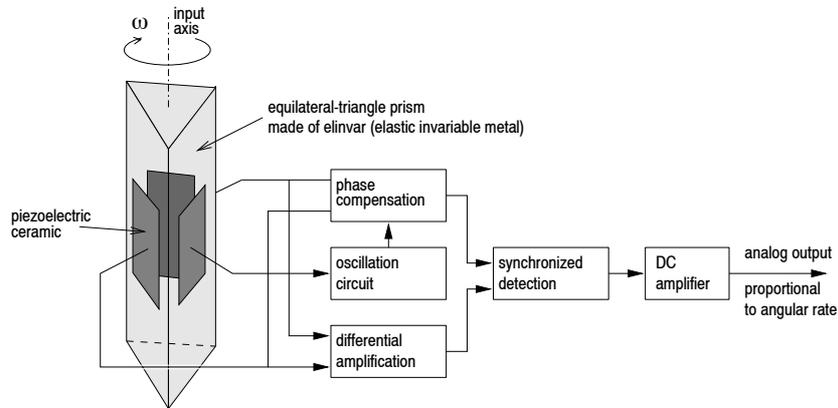

Figure 17. Piezoelectric vibrating prism gyroscope (adapted from [45]).

The Tuning Fork Gyroscope

The GyroChip sensor built by Systron Donner Inertial Division uses a a micro-miniature double-ended piezoelectric quartz tuning fork element. The sensor element and supporting structure are fabricated chemically from a single wafer of mono-crystalline piezoelectric quartz.

The drive times, being the active portion of the sensor, are driven by a high frequency oscillator circuit at a precise amplitude, producing the radial oscillation of the tines along the sensor plane, as shown in figure 18. A rotational motion about the sensor's longitudinal axis produces a DC voltage proportional to the rate of rotation due to the Coriolis forces acting on the sensing tines. Each tine will have a Coriolis force acting on it of:

$$F = 2m\varpi_i \times V_r \tag{15}$$

where m is the tine mass, V_r the instantaneous radial velocity and ϖ_i the input rate. This force is perpendicular to both the input rate and the instantaneous radial velocity.

The two drive tines move in opposite directions, and the resultant forces are perpendicular to the plane of the fork assembly, and also in opposite directions. This produces a torque which is proportional to the input rotational rate. Since the radial velocity is sinusoidal, the torque produced is also sinusoidal at the same frequency of the drive tines, and in-phase with the radial velocity of the tine.
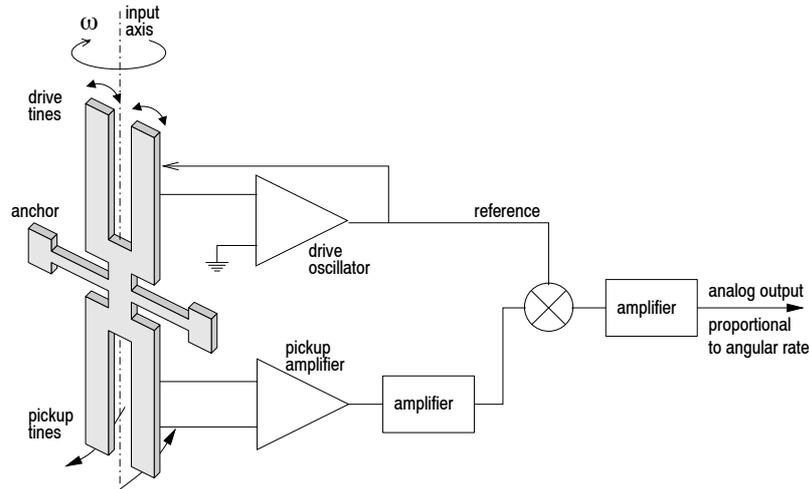
Figure 18. Example of tuning fork gyroscope (adapted from [46]).

The pickup tines respond to the oscillating torque by moving in and out of plane, producing a signal at the pickup amplifier. The sensed pickup signal is then synchronously demodulated to get the output signal proportional to the angular velocity along the sensor input axis.

Another interesting design of vibrating structure gyroscopes is the vibrating ring design used by British Aerospace Systems and Equipment, and Sumitomo Precision Products in their angular rate sensors. The sensor uses a micro-machined silicon ring placed over a permanent magnet. The ring is suspended by springs that allow it to vibrate and carry conducting wires to the ring. By applying an alternating current to the conductors on the ring, the micro-miniature ring is made to vibrate. By conveniently placing the driving and sensing conductors on the ring, the sensing ones will be subject to movement due to Coriolis forces. The sensing conductors in the ring, moving in a magnetic filed, produce an output proportional to that movement. The amplitude of this movement is determined by the sensor rotation rate. To increase linearity and dynamic range of the sensor, a closed loop feedback null voltage is applied to the sensing conductors. The ring is forced to its "rest" position and the null voltage demodulated to obtain a DC voltage proportional to the rotation rate of the sensor around it's sensing axis [42].

There are enumerate possible variations of the vibrating structure gyroscope and new micro-machined gyros are being developed, [47] is an example. As the micro-machinning technology improves, better and lower priced sensors are emerging.

4. Magnetic Compass

One good source for absolute orientation of mobile robots is the earth's magnetic field. However their accuracy is limited in the indoor environment or in situation when the earth's magnetic field is distorced. The magnetic compass has long been used in navigation. Mechanical magnetic compasses have evolved from the simple magnetised needle floating in water, to the more sophisticated and time proven systems in use today.

Much more practical and suitable for mobile robots are the fluxgate compasses. These saturable-core magnetometers use a gating action on AC-driven excitation coils to induce a time varying permeability in the sensor core, hence the name fluxgate. High permeability permeable materials present a lower magnetic resistance path and will draw in the lines of flux of an external uniform magnetic field. If the material is forced into saturation by

an additional magnetising force, the material will no longer affect the lines of flux of the external field. The fluxgate sensor uses this saturation phenomenon by driving the core element into and out of saturation, producing a time varying magnetic flux density that will induce e.m.f. changes in properly oriented sensing coils. Typical accuracy of fluxgate sensors in the absence of external disturbances of earth's magnetic field is $\pm 0.5 degrees$.

These variations will provide a measurement of the external DC magnetic field. See [2] for a more detailed description.

While the fluxgate sensor has been the predominat technology [2], magnetoresistive magnetomenters are replacing it some applications. Magnetoresistive materials change their resistance in the presence of a magnetic field. For sensing in the Earth's mangetic field range, the anisotropic magnetoresistive (AMR) sensor is used. AMR sensors typically employ a nickel-iron (Permalloy) thin film deposited onto a sillicon wafer to form the resistors. The circuit is arranged as a Wheatstone resistor bridge, as shown in figure 19a.
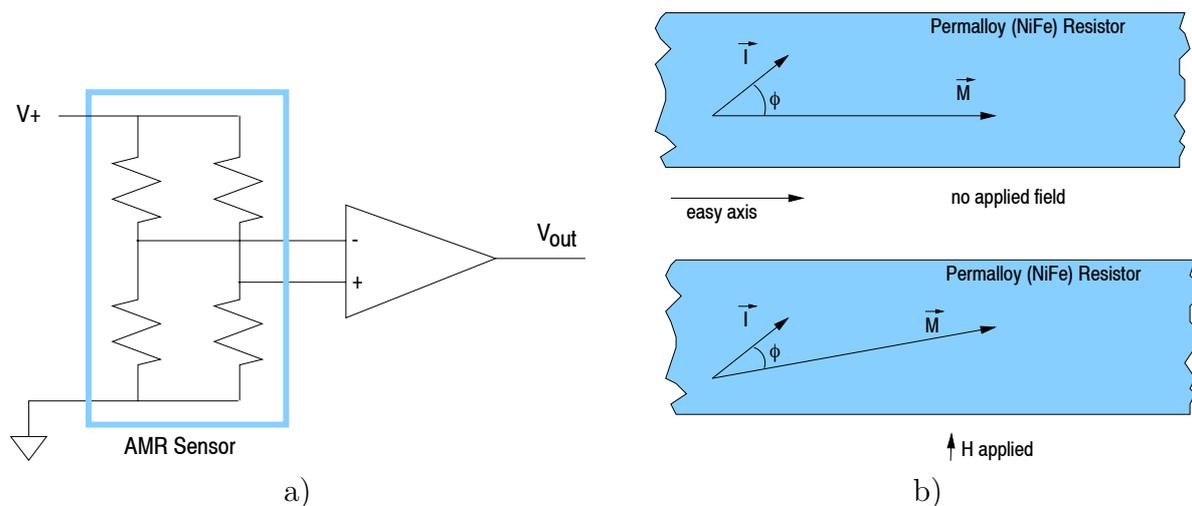

Figure 19. a) AMR sensor circuit; b) Magnetoresistive Effect (adapted from [48]).

The fabrication process ensures a preferred orientation, or easy axis, of the magnetization vector $\vec{M}$ along the lenght of the film. The film resistance is highest when the current flows parallel to $\vec{M}$, see figure 19b. This change in resistance is symetrical about the angle between the current $\vec{I}$ and $\vec{M}$, ϕ, and has a linear region around the 45-degree angle. The AMR sensors use a layout technique called barber pole biasing, where low resistance shorting bars are placed across the film width, to have the current flowing at a 45-degree angle. See [48] for more details. The reaction of the magnetoresistive effect is very fast and not limited by coils or oscillating frequencies. Typical AMR sensors have bandwidths in the range of 1-5MHz. AMR sensors are solid state, can be built on-chip and batch fabricated, allowing them to be auto-assembled with other circuit components. sensing coils. Typical accuracy of these sensors is $\pm 0.5 degrees$, with a resolution of $0.1 degrees$. AMR sensors are available from Philips, HL Planar and Honeywell.

5. Global Positioning System - GPS
5.1. Introduction
One of the most relevant external sensors, for outdoor applications, is the Global Positioning System (GPS). Navigation employing GPS and inertial sensors in a synergistic relationship and the integration of these two types of sensors not only overcomes performance issues found in each individual sensor, but could produce a system whose performance

exceeds that of the individual the sensors.

The inertial systems accuracy degrades with time, but GPS provides bounded accuracy.

5.2. Overview of the GPS system

The GPS system was designed for, and is operated by, the U. S. military. Its scope for military missions has been far outgrown with civilian applications, both commercial and scientific. The U. S. Department of Defence funds and controls the system, and civilian users world-wide can use the system free of charge and restrictions. However the accuracy is intentionally degraded for the non-military applications. The satellite-based systems can provide service to an unlimited number of users since the user receivers operate passively (i.e. receive only). The system provides continuous, high accuracy positioning anywhere on the surface of the planet and near space region, 24 hours a day, under all weather conditions. GPS also provides a form of co-ordinated universal time. The users receivers are small and lightweight, making hand-held global positioning systems a reality. See [49] for a brief history and description of the system or [50] for a more detailed description and underlying principles.

The GPS system is composed of three segments. The space segment consists of the GPS operational constellation of satellites. The constellation consists of 24 earth satellites, including 3 active spares, in 12 hour orbits. They are arranged in six orbital planes, separated by 60° in longitude, and inclined at about 55° to the equatorial plane. The satellites' nearly circular orbit, with an altitude of around $20000 km$, is such that they repeat exactly twice per sideral day. This implies that they repeat their ground track 4 minutes later each day. This constellation provides the user with between 5 and 8 satellites visible from any point on earth. The GPS requires a clear line of sight, and since the signals cannot penetrate water, soil, or walls very well, satellite visibility can be affected. The control segment consists of a world-wide system of tracking stations. A Master Control Station tracks the position of all satellites and maintains the overall system time standard. The other monitor stations measure signals from the satellites, allowing the Master Station to compute the satellites exact orbital parameters (ephemeris) and clock corrections, and upload them to the satellites, at least once a day. The satellite then sends subsets of this information to the user receivers. Satellites have redundant clocks, allowing them to maintain synchronous GPS system time. The user segment consists of the GPS receivers. They convert the satellite signals into position, velocity, and time estimates.

Position measurement is based on the principle of range triangulation. The receiver needs to know the range to the satellites and the positions of these satellites. The satellites positions can be determined by the ephemeris data broadcast from each satellite.

The ranges are determined by measuring the signal propagation time from each satellite to the receiver. For both, the receiver needs a local clock synchronised with the GPS system time. The atomic clock used in the satellites are impractical for the user receivers, and cheap crystal oscillators are used instead. These introduce a user clock bias that effectively adds a fourth unknown in the triangulation. The computed range to each satellite will be equally affected by the same clock bias dependent variable. These erroneous ranges are called pseudo-ranges. To determine position in three dimensions, four equations are needed to determine the four unknowns. For each satellite the following equation holds:

$$pseudorange_{sat_i} = \sqrt{(x - x_{sat_i})^2 + (y - y_{sat_i})^2 + (z - z_{sat_i})^2} + c\Delta t \qquad (16)$$
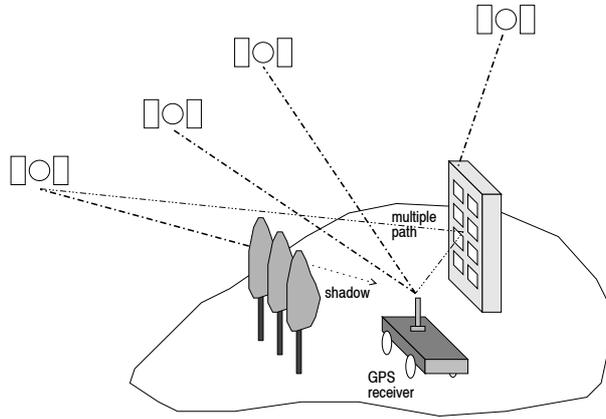
Figure 20. GPS basic idea.

where receiver and satellite positions are expressed in Cartesian geocentric co-ordinates, c is some constant, and Δt is the user clock bias, which it the same for every satellite, since the satellite clocks are synchronous [51]. Four satellites will be needed, and the three dimensional position will be given by the simultaneous solution(s) of the four equations. This is done in practice with a standard Newton-Raphson method for solving simultaneous non-linear equations. When more satellites are used, or some prior knowledge is available, a least squares technique is used. When altitude is known, navigation in two dimensions can be done with only three satellites.

All satellites broadcast two microwave carrier signals, L1 (1575.42 MHz) and L2 (1227.60 MHz), as well as UHF intra-satellite communications link, and S-band links to ground stations. The dual frequency approach allows estimation of ionospheric propagation delay at the receiver since the delay is frequency dependent. Satellites use unique Pseudo Random Noise (PRN) codes to modulate the signals, enabling satellite identification at the receiver end. The use of a particular type of PRN codes allows receivers with antenna only a few inches across to extract very low power signals from background noise by correlating them with expectations. The PRN codes of the different satellites are nearly uncorrelated with respect to each other, allowing receivers to "tune in" to different satellites by generating the appropriate PRN code and correlating with the received signal. The receiver computes satellite signal propagation time by shifting the self generated PRN code sequence in time, until the correlation function peaks. The time shift introduced gives the signal propagation time, including clock bias.

A precision code (the P-code) is modulated on to both L1 and L2 carriers. The P-code is a very long (seven days) 10 MHz PRN code. This means that acquisition of the P-code signal is slow unless the receiver position and/or time can be accurately initialised. To assist P-code acquisition a coarse acquisition code (the C/A-code) is assigned to each satellite. This 1 MHz PRN code repeats every 1023 bits (one millisecond) and is modulated onto the L1 carrier, in phase quadrature with the P-code signal. The Standard Positioning Service (SPS) available to all users is based on the C/A-code.

In the Anti-Spoofing (AS) mode of operation, the P-code is encrypted into the Y-code. This P(Y)-code requires a classified AS module, available only to authorised users with cryptographic keys, and is the basis for the Precise Positioning Service (PPS).

Navigation system data is modulated onto both carriers, using modulo-two addition to the PRN code modulation at a very low data rate [1]. This navigation message is a 50 Hz signal consisting of data bits that describe the GPS satellite orbits, clock corrections, and

other system parameters. The satellite's own precise ephemeris data is transmitted as well as less accurate ephemeris data for all satellites, known as the almanac. The navigation message is updated and repeated every 12.5 minutes.

5.3. GPS errors

Selective Availability (SA) is a deliberate error introduced to degrade system performance for non-U.S. military and government users. The system clocks and ephemeris data is degraded, adding uncertainty to the pseudo-range estimates. Since the SA bias, specific for each satellite, has low frequency terms in excess of a few hours, averaging pseudo-ranges estimates over short periods of time is not effective [52]. The potential accuracy of 30 meters for C/A code receivers is reduced to 100 meters.

Satellites are subject to deviations from their planned ephemeris, introducing ephemeris errors. The satellite clocks degrade over time, and if the ground control leaves then uncorrected, unwanted clock errors are introduced.

The troposphere (sea-level to $50\ km$) introduces propagation errors that are hard to model, unless local atmospheric data are available. The ionosphere ($50km$ to $5000km$) also introduces delays, and some compensation can be made with modeling based on almanac data. Dual frequency receivers allow direct estimation of ionospheric propagation delay since the delay is frequency dependent.

Shadows and multiple paths, as seen in figure 20, can also introduce errors. Shadows reduce the number of visible satellites available for positioning. Multiple path error is caused by reflected signals from surfaces near the receiver and can be difficult to detect and hard to avoid. The reflected signal can either interfere, or be mistaken for, the straight line path signal form the satellite.

The geometry of the satellites used for positioning will strongly affect how the pseudo-range error transforms into position error. Poor Geometric Dilution of Precision (GDOP) results when angles from the receiver to the set of used satellites are similar. The overlapping uncertainties of each satellite form a large volume uncertainty for receiver position. Good GDOP results when the angles are different and the overlapping uncertainty region is smaller.

5.4. Differential GPS (DGPS)

The basic idea behind differential positioning is to correct bias errors at the receiver with measured bias errors at a known nearby position. The reference receiver, knowing the satellites' ephemeris and the expected signal propagation delay, can calculate corrections for the measured transit times. This correction is computed for each visible satellite signal, and sent to the user receiver. These pseudo-range corrections can be radio broadcast to multiple user receivers. A more simplistic approach would be to simply correct the user position with the known position offset of the reference receiver. But this would only provide good corrections if both receivers where using the same set of satellites. Most of the above mentioned errors are overcome, although some like multipath and shadows remain (and to a certain extent tropospheric delays). Most importantly the Selective Availability error is cancelled, allowing typical positioning accuracy of around $100\ m$ to come down to $1 - 10\ m$. This means that a Standard Positioning Service (SPS) DGPS receiver has higher accuracy than a single Precise Positioning Service (PPS) GPS receiver, however the PPS receiver works standalone, and the SPS DGPS receiver needs a second receiver at a known location to provide differential data. DGPS performance degrades as the distance between the reference and user receiver increases, and is only suitable for distances under $100\ km$.

Another differential technique is the carrier-phase DGPS, also known as interferometric GPS, which bypasses the pseudo-random code and uses the high resolution carriers. The phase shift between signals received at the base and mobile units gives the signal path difference. It is also called code-less DGPS, as opposed to the coded DGPS where the pseudo-random noise code sequence is used to estimate signal path differences for each satellite. This technique is typically used in surveying applications, where accuracy of a few centimetres can be achieved. Besides the high cost, code-less DGPS requires a long set-up time, is subject to cycle slip, and unsuitable for fast moving vehicles.

6. Conclusions

Recent developments in sensor systems are providing the availability of devices with increasing performances, lower cost and smaller size. Micro-sensor technology, implemented in silicon has the ultimate potential to achieve integrated sensor systems combining absolute sensing with high dynamic performance in a miniature package, at a moderate cost.

References

[1] H.R. Everett, *Sensors for Mobile Robotics*, A.K. Peters, 1995, ISBN 1-56881-048-2.

[2] L. Feng, J. Borenstein, and H.R. Everett, "Where am I? - Sensors and Methods for Autonomous Mobile Robot Positioning," Tech. Rep. UM-MEAM-94-21, University of Michigan, December 1994.

[3] B.Ayruly and B. Barshan, "Identification of target primitives with multiple decision-making sonars using evidential reasoning," *Int. Journal of Robotics Research*, vol. 17, no. 16, pp. 598–623, June 1998.

[4] F. Moita, A. Feijão, U. Nunes, and A.T. de Almeida, "Ultrasonic and odometry modelling for mobile robots," in *Proc. European Robotics and Int. Systems Conf. (EURISCON94)*, 1994, pp. 337–346.

[5] P.J. Besl, "Active Optical Range Imaging Sensors," *Machine Vision and Applications*, vol. 1, no. 2, pp. 127–152, 1988.

[6] R.A. Jarvis, "A perspective on Range Finding Techniques for Computer Vision," *IEEE Trans. Pattern Analysis and Machine Intelligence*, vol. PAMI-5, no. 2, pp. 122–139, March 1983.

[7] B.T. Phong, "Illumination for computer generated pictures," *Commun. of the ACM*, vol. 18, no. 6, pp. 311–317, June 1975.

[8] L. Marques, D. Castro, U. Nunes, and A.T. de Almeida, "Optoelectronic Proximity Sensor for Robotics Applications," in *Proc. IEEE 8'th Mediterranean Electrotechnical Conf.*, 1996, pp. 1351–1354.

[9] Anita Flynn, "Redundant Sensors for Mobile Robot Navigation," Tech. Rep. 859, MIT Artificial Intelligence Laboratory, 1985.

[10] A.M. Flynn, "Combining Sonar and Infrared Sensors for Mobile Robot Navigation," *International Journal of Robotics Research*, vol. 7, no. 6, pp. 5–14, December 1988.

[11] Lino Marques, Urbano Nunes, and A.T. de Almeida, "Sensor Optoelectrónico Reflectivo com Potência de Emissão Variável e Detecção Digital," *Anais da Engenharia e Tecnologia Electrotécnica*, vol. 4, no. 7, pp. 64–68, Maio 1999.

[12] R.O. Duda, D. Nitzan, and P. Barret, "Use of Range and Reflectance Data to Find Planar Surface Regions," *IEEE Trans. Pattern Analysis and Machine Intelligence*, vol. PAMI-1, no. 3, pp. 259–271, July 1979.

[13] D. Nitzan, A.E. Brain, and R.O. Duda, "The Measurement and Use of Registered Re-

flectance and Range Data in Scene Analysis," *Proceedings of the IEEE*, vol. 65, no. 2, pp. 206–220, February 1977.

[14] R.A. Jarvis, "A Laser Time-of-Flight Range Scanner for Robotic Vision," *IEEE Trans. Pattern Analysis and Machine Intelligence*, vol. PAMI-5, no. 5, pp. 505–512, September 1983.

[15] D.C. Carmer and L.M. Peterson, "Laser Radar in Robotics," *Proceedings of the IEEE*, vol. 84, no. 2, pp. 299–320, February 1996.

[16] D.J. Conrad and R.E. Sampson, "3D Range Imaging Sensors," in *Traditional and Non-Traditional Robotic Sensors*, T.C. Henderson, Ed., vol. F63 of *NATO ASI Series*, pp. 35–48. Springer-Verlag, Berlin, 1990.

[17] P.M. Will and K.S. Pennington, "Grid Coding: A Novel Technique for Image Processing," *Proceedings of the IEEE*, vol. 60, no. 6, pp. 669–680, June 1972.

[18] G.C. Stockman, S.W. Chen, G. Hu, and N. Shrikhande, "Sensing and Recognition of Rigid Objects Using Structured Light," *IEEE Control Systems Magazine*, vol. 8, no. 6, pp. 14–22, June 1988.

[19] S.M. Dunn, R.L. Keizer, and J. Yu, "Measuring the Area and Volume of the Human Body with Structured Light," *IEEE Trans. Systems, Man and Cybernetics*, vol. SMC-19, no. 6, pp. 1350–1364, November 1989.

[20] Y.F. Wang, "Characterizing Three-Dimensional Surface Structures from Visual Images," *IEEE Trans. Pattern Analysis and Machine Intelligence*, vol. PAMI-13, no. 1, pp. 52–60, January 1991.

[21] M.D. Altschuler et al., "Robot Vision by Encoded Light Beams," in *Three-dimensional machine vision*, Takeo Kanade, Ed., pp. 97–149. Kluwer Academic Publishers, Boston, 1987.

[22] P. Vuylsteke and A. Oosterlinck, "Range Image Acquisition with a Single Binary-Encoded Light Pattern," *IEEE Trans. Pattern Analysis and Machine Intelligence*, vol. PAMI-12, no. 12, pp. 148–164, Feb 1990.

[23] K.L. Boyer and A.C. Kak, "Color-Encoded Structured Light for Rapid Active Ranging," *IEEE Trans. Pattern Analysis and Machine Intelligence*, vol. PAMI-9, no. 1, pp. 14–28, January 1987.

[24] C. Wust and D.W. Capson, "Surface Profile Measurement Using Color Frinje Projection," *Machine Vision and Applications*, vol. 4, pp. 193–203, 1991.

[25] Maruyama and S. Abe, "Range Sensing by Projecting Multiple Slits with Random Cuts," *IEEE Trans. Pattern Analysis and Machine Intelligence*, vol. PAMI-15, no. 16, pp. 647–651, Jun 1993.

[26] P. Vuylsteke, C.B. Price, and A. Oosterlinck, "Image Sensors for Real-Time 3D Acquisition: Part 1," in *Traditional and Non-Traditional Robotic Sensors*, T.C. Henderson, Ed., vol. F63 of *NATO ASI Series*, pp. 187–210. Springer-Verlag, Berlin, 1990.

[27] E. Mouaddib, J. Battle, and J. Salvi, "Recent Progress in Structured Light in order to Solve the Correspondence Problem in Stereo Vision," in *Proc. IEEE Conf. on Robotics and Automation*, 1997, pp. 130–136.

[28] L. Marques, U. Nunes, and A. T. de Almeida, "A New 3D Optical Triangulation Sensor for Robotics," in *Proc. 5th Int. Workshop on Advanced Motion Control*, 1998, pp. 512–517.

[29] L. Marques, U. Nunes, and A. T. de Almeida, "Opto3D: A New Distance and Orientation Sensor for Robotics," in *Proc. 9th Int. Conf. on Sensors Transducers & Systems (SENSOR99)*, 1999, pp. 445–450.

[30] S. Lee and J. Desai, "Implementation and Evaluation of HexEYE: A Distributed Optical Proximity Sensor System," in *Proc. IEEE Conf. on Robotics and Automation*, 1995, pp. 2353–2360.

[31] T. Kanade and M. Fuhrman, "A Noncontact Optical Proximity Sensor for Measuring

Surface Shape," in *Three-dimensional machine vision*, Takeo Kanade, Ed., pp. 151–192. Kluwer Academic Publishers, Boston, 1987.

[32] Yalin Xiong and Steven A. Shafer, "Depth from Focusing and Defocusing," Tech. Rep. 93-07, The Robotics Institute - Carnegie Mellon University, 1993.

[33] S.K. Nayar, M. Watanabe, and M. Noguchi, "Real-Time Focus Range Sensor," *IEEE Trans. Pattern Analysis and Machine Intelligence*, vol. PAMI-18, no. 12, pp. 1186–1198, Dec 1996.

[34] T. Viéville and O.D. Faugeras, "Computation of Inertial Information on a Robot," in *Fifth International Symposium on Robotics Research*, Hirofumi Miura and Suguru Arimoto, Eds. 1989, pp. 57–65, MIT-Press.

[35] R.P.G. Collinson, *Introduction to Avionics*, Chapman & Hall, 1996, ISBN 0-412-48250-9.

[36] John M. Slater, *Principles of Operation of Inertial Sensing Devices*, pp. 47–71, George R. Pitman (ed.), John Wiley & Sons, 1962.

[37] Morris M. Kuritsky and Murray S. Goldstein, *Inertial Navigation*, pp. 96–116, T. Lozano-Perez (ed), Springer-Verlag New York, 1990.

[38] Henry V. Allen, Stephen C. Terry, and James W. Knutti, "Understanding Silicon Accelerometers," *Sensors*, September 1989.

[39] ICSensors, *Silicon Accelerometers*, January 1988, Technical Note TN-008.

[40] Summit Instruments, *34100A Theory of Operation*, September 1994, Technical Note 402.

[41] Analog Devices, *ADXL05*, 1996, Datasheet.

[42] British Aerospace Systems and Equipment, Sumitomo Precision Products, *Motion Sensors*, 1996, Product Literature.

[43] B. Barshan and H. Durrant-Whyte, "Inertial Navigation Systems for Mobile Robots," *IEEE Transactions on Robotics and Automation*, vol. 11, no. 3, pp. 328–342, June 1995.

[44] Kiyoshi Komoriya and Eimei Oyama, "Position Estimation of a Mobile Robot Using Optical Fiber Gyroscope (OFG)," in *Proceedings of the 1994 IEEE International Conference on Intelligent Robots and Systems*, 1994, pp. 143–149.

[45] Murata, *Piezoelectric Vibrating Gyroscope GYROSTAR*, 1991, Cat. No. S34E-1.

[46] Systron Donner Inertial Division, *GyroChip*, 1995, Product Literature.

[47] William A. Clark, Roger T. Howe, and Roberto Horowitz, "Surface Micromachined Z-axis Vibratory Rate Gyroscope," in *Tech. Dig. Solid-State Sensor and Actuator Workshop*, June 1996, pp. 283–287.

[48] Michael J. Caruso, Tamra Bratland, Carl H. Smith, and Robert Schneider, "A New Perspective on Magnetic Field Sensing," Tech. Rep., Honeywell, Inc, 1998.

[49] Ivan A. Getting, "The Global Positioning System," *IEEE Spectrum*, pp. 236–247, December 1993.

[50] Elliott D. Kaplan, *Understanding GPS: Principles and Applications*, Artech House, 1996, ISBN 0-89006-793-7.

[51] Alonzo Kelly, "Modern Inertial and Satellite Navigation Systems," Tech. Rep. CMU-RI-TR-94-15, Carnegie Mellon University, May 1994.

[52] Peter H. Dana, "Global Positioning System Overview," Tech. Rep. CMU-RI-TR-94-15, Department of Geography, University of Texas at Austin, http://www.utexas.edu/depts/grg/gcraft/notes/gps/gps.html, 1997.